THE JOURNAL OF PHYSICAL CHEMISTRY A
A JOURNAL OF THE AMERICAN CHEMICAL SOCIETY

pubs.acs.org/JPCA Article

# Photoelectron Spectroscopy of Size-Selected Bismuth−Boron Clusters: $BiB_n^-$ ($n$ = 6−8)

*Published as part of The Journal of Physical Chemistry virtual special issue "125 Years of The Journal of Physical Chemistry".*

Wei-Jia Chen, Maksim Kulichenko, Hyun Wook Choi, Joseph Cavanagh, Dao-Fu Yuan,* Alexander I. Boldyrev,* and Lai-Sheng Wang*

Cite This: *J. Phys. Chem. A* 2021, 125, 6751−6760 Read Online

ACCESS | Metrics & More | Article Recommendations | Supporting Information

**ABSTRACT:** Because of its low toxicity, bismuth is considered to be a "green metal" and has received increasing attention in chemistry and materials science. To understand the chemical bonding of bismuth, here we report a joint experimental and theoretical study on a series of bismuth-doped boron clusters, $BiB_n^-$ ($n$ = 6−8). Well-resolved photoelectron spectra are obtained and are used to understand the structures and bonding of $BiB_n^-$ in conjunction with theoretical calculations. Global minimum searches find that all three $BiB_n^-$ clusters have planar structures with the Bi atom bonded to the edge of the planar $B_n$ moiety via two Bi−B $\sigma$ bonds as well as $\pi$ bonding by the $6p_z$ orbital. $BiB_6^-$ is found to consist of a double-chain $B_6$ with a terminal Bi atom. Both $BiB_7^-$ and $BiB_8^-$ are composed of a Bi atom bonded to the planar global minima of the $B_7^-$ and $B_8^-$ clusters. Chemical bonding analyses reveal that $BiB_6^-$ is doubly antiaromatic, whereas $BiB_7^-$ and $BiB_8^-$ are doubly aromatic. In the neutral $BiB_n$ ($n$ = 6−8) clusters, except $BiB_6$ which has a planar structure similar to the anion, the global minima of both $BiB_7$ and $BiB_8$ are found to be half-sandwich-type structures due to the high stability of the doubly aromatic $B_7^{3-}$ and $B_8^{2-}$ molecular wheel ligands.

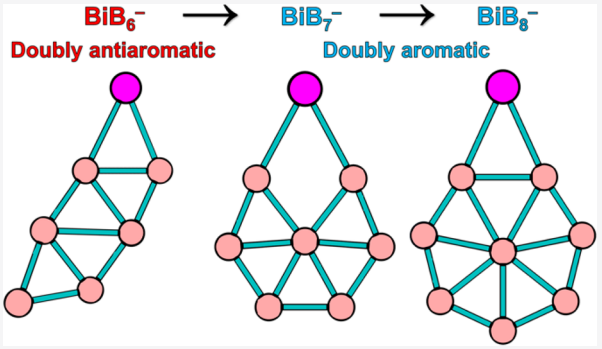


## 1. INTRODUCTION

The electron deficiency of boron results in a variety of bulk allotropes and compounds consisting of different three-dimensional (3D) cages.[1−4] Over the past two decades, extensive research has been conducted on size-selected boron clusters using joint experimental and first-principle theoretical studies.[5−10] Different from the bulk, small boron clusters have been found to process predominantly two-dimensional (2D) structures consisting of $B_3$ triangles decorated with tetragonal, pentagonal, or hexagonal holes.[7−9] One of the most interesting 2D boron clusters is the $C_{6v}$ $B_{36}$ cluster with a central hexagonal hole, providing the first experimental evidence of the viability of atom-thin 2D boron (borophene).[11] Borophenes have been realized on metal substrates,[12,13] becoming a new class of synthetic 2D materials. The $B_{40}$ cluster was found to have a cage structure marking the discovery of the first all-boron fullerene (borospherene),[14] while the $B_{48}^-$ cluster with a bilayer structure was the largest bare boron cluster interrogated experimentally up to date.[15] Numerous metal-doped boron clusters have also been produced and studied, significantly expanding the structural diversity of nanoborons. The study on transition-metal-doped boron clusters revealed the existence of various structures including metal-centered borometallic molecular wheels,[16−18] metallo-boronanotubes,[19] and metallo-borophenes.[20,21] The $PrB_7^-$ cluster contains a half-sandwich structure featuring a $B_7^{3-}$ moiety,[22] which was also found recently in $B_9O^-$.[23] Dilanthanide boron clusters were found to form inverse sandwiches,[24,25] while $La_3B_{18}^-$ features the first spherical trihedral metallo-borospherene.[26]

Bismuth is the heaviest stable metal element in the periodic table, but it has low toxicity relative to its neighbors.[27] In fact, bismuth is considered a "green metal", and it has received increasing attention in chemistry, materials science, and medicinal chemistry.[28−30] Being a heavy member of the important III−V semiconductor family, bismuth boride has unique electronic and optical properties with significant potentials for industrial applications.[31−33] However, bulk bismuth borides have not been synthesized. Because of their large size discrepancy, the bismuth−boron bond is expected to

Received: June 30, 2021
Revised: July 24, 2021
Published: August 2, 2021







https://doi.org/10.1021/acs.jpca.1c05846
J. Phys. Chem. A 2021, 125, 6751−6760

be weak, although very little is known. Only recently have a series of studies focusing on the bismuth−boron bonding been reported in $BiBO^-$, $Bi_2B^-$, and $BiB_2O^-$, which are found to contain a single Bi−B, double Bi═B, and triple Bi≡B bond, respectively.[34,35] Other than that, there have been few experimental studies on bismuth−boron species except a recent investigation on the dibismuth boride clusters of $Bi_2B_n^-$ ($n$ = 2−4).[36]

Bismuth−boron clusters are not only ideal systems to probe the chemical bonding between Bi and B, they will also lay the foundation to synthesize bulk bismuth borides or new bismuth−boron nanostructures. In the current work, we report a joint photoelectron spectroscopy (PES) and theoretical study on a series of bismuth-doped boron clusters, $BiB_n^-$ ($n$ = 6−8). Well-resolved photoelectron spectra are obtained for all three clusters and are combined with theoretical calculations to elucidate their structures and bonding. The global minima of the $BiB_n^-$ ($n$ = 6−8) clusters are all found to have 2D structures featuring a Bi atom bonded to the edge of a planar $B_n$ motif. Chemical bonding analyses show that the elongated $BiB_6^-$ cluster is doubly antiaromatic, while both $BiB_7^-$ and $BiB_8^-$ are doubly aromatic. Interestingly, the global minima of neutral $BiB_7$ and $BiB_8$ are three-dimensional (3D) half-sandwich-type structures as a result of the high stability and aromaticity of the $B_7^{3-}$ and $B_8^{2-}$ molecular wheel motifs.

## 2. EXPERIMENTAL AND THEORETICAL METHODS

**2.1. Photoelectron Spectroscopy.** The experiment was conducted by using a magnetic-bottle PES apparatus equipped with a laser-vaporization supersonic cluster source, the details of which have been published elsewhere.[8,37] The $BiB_n^-$ ($n$ = 6−8) clusters were produced by laser vaporization of a disk target prepared by mixing powders of bismuth and $^{11}$B-enriched boron (1/1 Bi/B molar ratio). The laser-induced plasma was cooled by a high-pressure He carrier gas seeded with 5% Ar, initiating nucleation and cluster formation. The nascent clusters were entrained by the carrier gas and underwent a supersonic expansion to produce a cold cluster beam. The cluster temperature was expected to be below room temperature[38] and could be varied slightly by controlling the resident time of the cluster in the nozzle.[8] The Ar-seeded helium carrier was found to be better for cooling heavier clusters, as demonstrated previously by the observation of Ar-tagged $Au_x^-$ clusters.[39] After passing a skimmer, anionic clusters were extracted from the collimated cluster beam and analyzed by time-of-flight mass spectrometry. The clusters of interest were mass-selected and decelerated before photodetachment by a laser beam from the fourth harmonic of a Nd:YAG laser at 266 nm (4.661 eV). Photoelectrons were collected at nearly 100% efficiency by the magnetic bottle and analyzed in a 3.5 m long electron flight tube. The photoelectron kinetic energy ($E_k$) was calibrated by using the known spectrum of $Bi^-$. The resolution of the magnetic-bottle photoelectron analyzer was $\Delta E_k/E_k \approx 2.5\%$, that is, ∼25 meV for 1 eV electrons.

**2.2. Theoretical Methods.** Global minimum searches were performed by using the AFFCK code, which was an efficient global optimization method through the introduction of an intermediate step where structures were optimized by using a classical force field generated on the fly within the algorithm.[40] About 1300 starting geometries were generated for $BiB_6^-$ and ∼2000 for $BiB_7^-$ and $BiB_8^-$. After the initial optimization at the PBE0/LANL2DZ level,[41] the low-lying isomers were reoptimized at the PBE0/aug-cc-pVTZlevel of theory (with the effective core potential for Bi)[42] as implemented in Gaussian-16.[43] Both singlet and triplet states for $BiB_6^-$ and $BiB_8^-$, and doublet and quartet states for $BiB_7^-$, were tested for each generated structure. The one-determinant character of the global minimum wave functions was examined by the wave function stability test (stable = opt).

Vertical detachment energies (VDEs) and adiabatic detachment energies (ADEs) were calculated by using two approaches: (1) time-dependent DFT (TD-DFT) at the PBE0/aug-cc-pVTZ level of theory and (2) CCSD(T)/def2-TZVP.[44,45] The first vertical detachment energy ($VDE_1$) was calculated as the energy difference between the neutral and anion at the optimized anion geometry. The ADE was computed by using the optimized anion and the optimized neutral for the corresponding anion structure. Spin−orbit effects were not treated explicitly in the current work, which might affect the accuracy of the computed detachment energies. However, the overall agreement between the theoretical VDEs and the experimental spectral patterns is quite good, as shown below.

The adaptive natural density partitioning (AdNDP) method[46,47] was used for the chemical bonding analyses as a time-proven probe for deciphering delocalized bonding in various chemical systems.[48−55] The algorithm works within a concept of occupation numbers (ONs), such that the closer an ON of a certain bond is to 2.0 (1.0 for single-electron bonds), the more reliable the bonding picture is.

## 3. PHOTOELECTRON SPECTRA OF $BIB_n^-$ ($n$ = 6−8)

The photoelectron spectra of $BiB_n^-$ at 266 nm are shown in Figures 1−3 for $n$ = 6−8, respectively. The observed PES

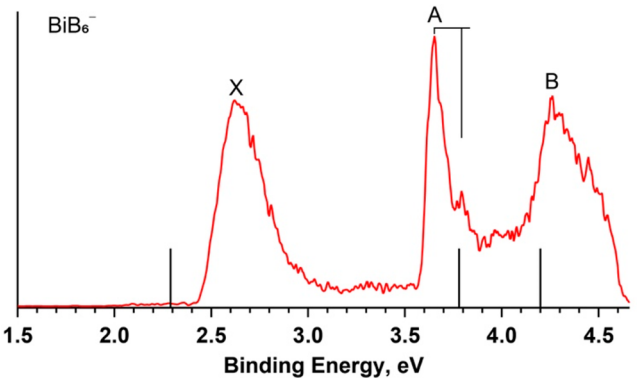


**Figure 1.** Photoelectron spectrum of $BiB_6^-$ at 266 nm (4.661 eV). The vertical bars correspond to computed VDEs at the PBE0/aug-cc-pVTZ level of theory.

bands are labeled with letters (X, A, B, ...), and the detailed VDEs are shown in Tables 1−3, along with their theoretical VDEs and electron configurations. In each spectrum, band X

**Table 1. Experimental VDEs and Comparison with the Calculated Values for the Global Minimum of $BiB_6^-$**

| band | VDE (exptl) | final state and electron configuration | VDE (theor) PBE0/aug-cc-pVTZ |
|---|---|---|---|
| X | 2.62 ± 0.03 | $^2$A {...(25a)$^2$(26a)$^2$(27a)$^1$} | 2.29 |
| A | 3.65 ± 0.02 | $^2$A {...(25a)$^2$(26a)$^1$(27a)$^2$} | 3.78 |
| B | 4.26 ± 0.03 | $^2$A {...(25a)$^1$(26a)$^2$(27a)$^2$} | 4.20 |



https://doi.org/10.1021/acs.jpca.1c05846
J. Phys. Chem. A 2021, 125, 6751−6760

represents the transition from the anionic ground state to the electronic ground state of the corresponding neutral, while bands A, B, ... indicate transitions from the anionic ground state to excited states of the corresponding neutral species.

**3.1. $BiB_6^-$.** The photoelectron spectrum of $BiB_6^-$ displays three well-resolved bands, as shown in Figure 1. Band X gives rise to the first VDE at 2.62 eV. The ADE is estimated to be 2.46 ± 0.04 eV from its onset, which also represents the electron affinity (EA) of the corresponding neutral $BiB_6$. Following a large energy gap, band A at 3.65 eV is intense and sharp with a short vibrational progression and a vibrational spacing of ~1120 $cm^{-1}$. A broad band B is observed at 4.26 eV.

**3.2. $BiB_7^-$.** The photoelectron spectrum of $BiB_7^-$ (Figure 2) is congested with more complicated features because it is

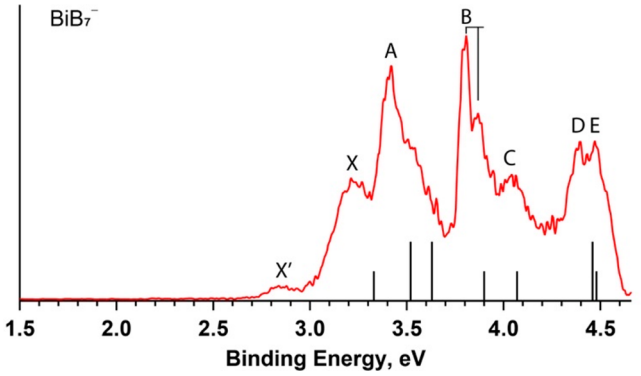


**Figure 2.** Photoelectron spectrum of $BiB_7^-$ at 266 nm (4.661 eV). The vertical bars correspond to computed VDEs at the PBE0/aug-cc-pVTZ level of theory. The longer bars correspond to transitions to triplet final states; the shorter bars correspond to transitions to singlet final states.

open-shell. The strong band X is broad, yielding a VDE of 3.21 eV and an estimated ADE of 3.03 ± 0.06 eV. A broad band A with an unresolved shoulder closely follows band X at a VDE of 3.42 eV. Band B at 3.81 eV is sharp, and it contains a short vibrational progression with a spacing of ~490 $cm^{-1}$. A weaker and broad band C is observed with a VDE of 4.04 eV. At the high binding energy side, two closely spaced bands, D and E, are observed at 4.39 and 4.47 eV, respectively. The weak band X′ on the low binding energy side at 2.84 eV is likely from a low-lying isomer.

**3.3. $BiB_8^-$.** The photoelectron spectrum of $BiB_8^-$ displays a relatively simple spectral pattern with three well-resolved bands, as shown in Figure 3. The sharp band X yields a VDE of

**Table 2. Experimental VDEs and Comparison with the Calculated Values for the Global Minimum of $BiB_7^-$**

| band | VDE (exptl) | final state and electron configuration | VDE (theor) PBE0/aug-cc-pVTZ |
|---|---|---|---|
| X | 3.21 ± 0.03 | $^1A_2$ {...$(15a_1)^2(9b_2)^2(4b_1)^2(2a_2)^0$} | 3.33 |
| A | 3.42 ± 0.03 | $^3B_1$ {...$(15a_1)^2(9b_2)^2(4b_1)^1(2a_2)^1$} | 3.52 |
| | ~3.5[a] | $^3B_2$ {...$(15a_1)^2(9b_2)^1(4b_1)^2(2a_2)^1$} | 3.63 |
| B | 3.81 ± 0.02 | $^1B_1$ {...$(15a_1)^2(9b_2)^2(4b_1)^1(2a_2)^1$} | 3.90 |
| C | 4.04 ± 0.03 | $^1B_2$ {...$(15a_1)^2(9b_2)^1(4b_1)^2(2a_2)^1$} | 4.07 |
| D | 4.39 ± 0.02 | $^3A_1$ {...$(15a_1)^1(9b_2)^2(4b_1)^2(2a_2)^1$} | 4.46 |
| E | 4.47 ± 0.02 | $^1A_1$ {...$(15a_1)^1(9b_2)^2(4b_1)^2(2a_2)^1$} | 4.48 |

[a]The unresolved shoulder of band A (see Figure 2).

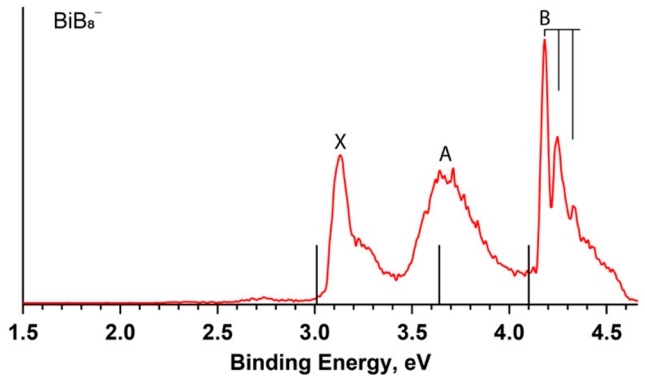


**Figure 3.** Photoelectron spectrum of $BiB_8^-$ at 266 nm (4.661 eV). The vertical bars correspond to computed VDEs at the PBE0/aug-cc-pVTZ level of theory.

3.13 eV and an ADE of 3.07 ± 0.03 eV. The shoulder on the high binding energy side of band X is likely an unresolved vibrational peak. A relatively broad band A is observed at 3.64 eV. The intense and sharp band B gives a VDE of 4.18 eV and a vibrational progression with a frequency of 570 $cm^{-1}$. There were very weak signals at the low binding energy side around ~2.7 eV (not labeled), which could be due to a low-lying isomer.

## 4. THEORETICAL RESULTS

The global minima of $BiB_n^-$ ($n$ = 6−8) along with several low-lying isomers are displayed in Figure 4. More low-lying structures are given in Figure S1.

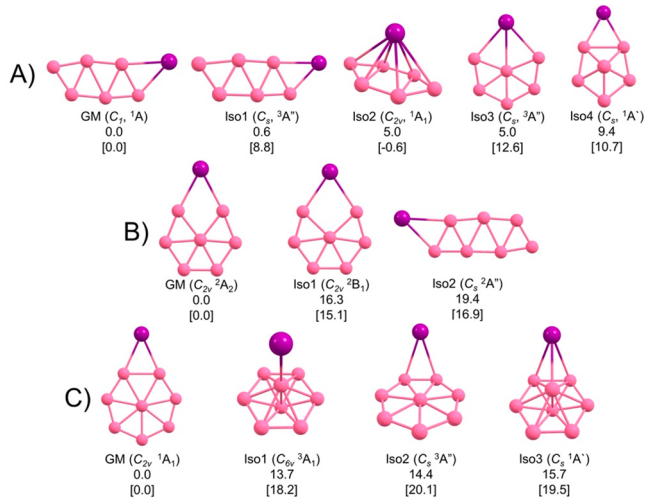


**Figure 4.** Global minima and low-lying isomers of (A) $BiB_6^-$, (B) $BiB_7^-$, and (C) $BiB_8^-$. Relative energies are given in kcal/mol at the PBE0/aug-cc-pVTZ + ZPE level and the CCSD(T)/def2-TZVP level [in brackets].

**4.1. $BiB_6^-$.** The global minimum of $BiB_6^-$ was found to be a closed-shell 2D structure with $C_1$ symmetry ($^1$A, Figure 4A) at the PBE0 level. The $B_6$ motif is similar to the global minimum of the bare $B_6$ cluster with some in-plane distortions.[56] The valence MOs for the $C_1$ $BiB_6^-$ are displayed in Figure S2. The HOMO−LUMO gap is computed to be 2 eV at the PBE0/aug-cc-pVTZ level, indicating the global minimum of $BiB_6^-$ is a stable electronic system. The first low-lying isomer (Iso1) can be considered as the triplet excited state of the global


https://doi.org/10.1021/acs.jpca.1c05846
J. Phys. Chem. A 2021, 125, 6751−6760

minimum. It is almost degenerate with the global minimum at the PBE0 level but is much higher in energy at the CCSD(T) level. The second low-lying isomer (Iso2) is a 3D half-sandwich type structure, which is 5.0 kcal/mol higher in energy at the PBE0 level but becomes even lower in energy than the $C_1$ 2D global minimum. Clearly, the true global minimum can only be determined by comparison with the experimental data. The ADE and $VDE_1$ for the global minimum of $BiB_6^-$, as well as the $VDE_1$ for Iso1 and Iso2, are calculated at two different levels of theory, as shown in Table 4. Higher VDEs at the TD-DFT level for the $C_1$ 2D global minimum are given in Table 1, where they are compared with the experimental data.

**Table 3. Experimental VDEs and Comparison with the Calculated Values for the Global Minimum of $BiB_8^-$**

| band | VDE (exptl) | final state and electron configuration | VDE (theor) PBE0/aug-cc-pVTZ |
|---|---|---|---|
| X | 3.13 ± 0.02 | $^2A_2$ $\{...(4b_1)^2(10b_2)^2(2a_2)^1\}$ | 3.01 |
| A | 3.64 ± 0.03 | $^2B_2$ $\{...(4b_1)^2(10b_2)^1(2a_2)^2\}$ | 3.78 |
| B | 4.18 ± 0.02 | $^2B_1$ $\{...(4b_1)^1(10b_2)^2(2a_2)^2\}$ | 4.10 |

**4.2. $BiB_7^-$.** The global minimum of $BiB_7^-$ is a doublet $C_{2v}$ ($^2A_2$) planar structure with the Bi atom bonded to the periphery of a hexagonal $B_7$ cluster (Figure 4B). The $B_7$ motif is similar to the global minimum of the bare $B_7$ except that the latter is only quasi-planar.[57] The valence MOs of the global minimum are shown in Figure S3. The HOMO−SOMO (beta MOs) gap was computed to be 2.6 eV, and the SOMO−LUMO gap (alpha MOs) was 3.2 eV. The next low-lying isomer (Iso1) is 15.1 kcal/mol higher in energy at the CCSD(T) level ($C_{2v}$, $^2B_1$, Figure 4B), and its structure is similar to the global minimum except that the $B_7$ moiety undergoes some in-plane distortions. In fact, Iso1 can be viewed as replacing a B atom with the Bi atom on the periphery of the $B_8^-$ cluster.[58] Clearly, the insertion of the Bi atom is too disruptive to the B−B bonding, resulting in a much higher energy Iso1. The second low-lying isomer has an elongated double-chain structure, similar to the global minimum of $BiB_6^-$, but it is significantly higher in energy in comparison to the $C_{2v}$ global minimum. The computed ADE and $VDE_1$ for the global minimum and the $VDE_1$ for Iso1 of $BiB_7^-$ at both PBE0 and CCSD(T) are also given in Table 4. The higher VDEs of the global minimum at the TD-DFT level are compared with the experimental data in Table 2.

**4.3. $BiB_8^-$.** The global minimum of $BiB_8^-$ consists of a $B_8$ wheel and a Bi atom bonded to its edge with $C_{2v}$ symmetry (Figure 4C). The $B_8$ motif is similar to the global minimum of the bare $B_8$ cluster.[58] The valence MOs for the global minimum are shown in Figure S4. The HOMO−LUMO gap was computed to be 2.37 eV. The first low-lying isomer (Iso1) is a 3D bipyramidal structure with a triplet state and $C_{6v}$ symmetry. It is 13.7 kcal/mol higher in energy than the planar global minimum at the PBE0 level and 18.2 kcal/mol higher at the CCSD(T) level. The second low-lying isomer is a triplet $C_s$ structure with the Bi atom bent out of the $B_8$ plane. Another 3D bipyramidal structure (Iso3) is close in energy to Iso2. The computed ADE and $VDE_1$ for the global minimum as well as the computed $VDE_1$ for the three low-lying isomers of $BiB_8^-$ are also given in Table 4. The higher VDEs of the global minimum at the TD-DFT level are compared with the experimental data in Table 3.

**4.4. Neutral $BiB_n$ ($n$ = 6−8).** We also performed global minimum searches for neutral $BiB_n$ ($n$ = 6−8), as shown in Figure 5. The potential energy surfaces of the neutral clusters are found to be quite different from those of the anions. While the global minimum of neutral $BiB_6$ is similar to that of the

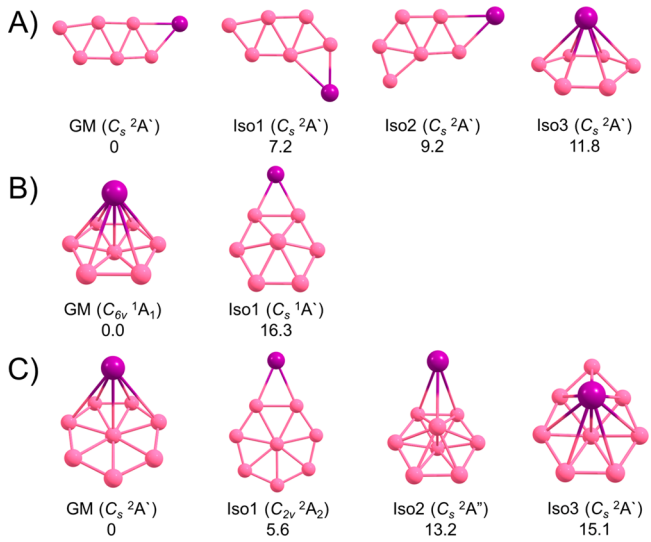


**Figure 5.** Low-lying isomers of (A) $BiB_6$, (B) $BiB_7$, and (C) $BiB_8$. Relative energies are given in kcal/mol at the PBE0/aug-cc-pVTZ + ZPE level of theory.

**Table 4. Comparison of the Experimental ADE and $VDE_1$ with Calculated Values at the PBE0/aug-cc-pVTZ and CCSD(T)/def2-TZVP Levels of Theory for the Global Minima (GM) of $BiB_n^-$ ($n$ = 6−8) and the $VDE_1$ for Low-Lying Isomers**

| | | ADE (theor) | | $VDE_1$ (theor) | | | |
|---|---|---|---|---|---|---|---|
| | final state | PBE0 | CCSD(T) | PBE0 | CCSD(T) | ADE (exptl) | $VDE_1$ (exptl) |
| $BiB_6^-$, $C_1$ (GM) | $^2A$ | 2.15 | 2.34 | 2.29 | 2.53 | 2.46 | 2.62 |
| $C_s$ (Iso1) | $^2A'$ | | | 2.21 | 2.07 | | |
| $C_{2v}$ (Iso2) | $^2B_2$ | | | 2.61 | 3.02 | | |
| $BiB_7^-$, $C_{2v}$ (GM) | $^1A_1$ | 2.86 | 2.75 | 3.33 | 3.18 | 3.03 | 3.21 |
| $C_{2v}$ (Iso1) | $^1B_2$ | | | 2.77 | 2.83 | 2.71 | 2.84 |
| $BiB_8^-$, $C_{2v}$ (GM) | $^2A_2$ | 2.94 | 3.13 | 3.01 | 3.19 | 3.07 | 3.13 |
| $C_{6v}$ (Iso1) | $^2E_1$ | | | 3.65 | 3.78 | | |
| $C_s$ (Iso2) | $^2A'$ | | | 2.78 | 2.74 | | ~2.7[a] |
| $C_s$ (Iso3) | $^2A''$ | | | 2.78 | 2.88 | | |

[a]The weak low-binding energy feature in Figure 3.



https://doi.org/10.1021/acs.jpca.1c05846
J. Phys. Chem. A 2021, 125, 6751−6760

anion, the Iso1 and Iso2 of the neutral are not present as low-lying isomers in the anion (Figure 4). More remarkably, the global minima of $BiB_7$ and $BiB_8$ are 3D half-sandwich type structures, in which the $B_7$ and $B_8$ motifs are similar to the global minima of the respective bare clusters.[57,58] The planar global minimum structures of the anions become Iso1 for both neutral $BiB_7$ and $BiB_8$. It is interesting to see that detachment of a single electron can significantly alter the relative stability of the different isomers of these clusters. The coordinates of the global minima of the $BiB_n^-$ ($n$ = 6−8) anions and the $BiB_n$ neutrals at the PBE0 level are given in Tables S1−S6.

## 5. DISCUSSION

**5.1. Comparison between Experiment and Theory.** The experimental PES data are essential for the verification and determination of the global minima and low-lying isomers of size-selected clusters. The computed ADE/$VDE_1$ for the global minima of $BiB_n^-$ ($n$ = 6−8) and $VDE_1$ for low-lying isomers are compared with the experimental results in Table 4. The calculated VDEs for all the detachment channels of the global minima within the experimentally observed spectral range are compared with the PES data in Tables 1−3 and indicated in Figures 1−3.

*5.1.1. $BiB_6^-$.* The calculated ADE/$VDE_1$ of 2.34/2.53 eV for the global minimum of $BiB_6^-$ at the CCSD(T) level agrees well with the experimental data of 2.46/2.62 eV, while the values calculated at the PBE0 level (2.15/2.29 eV) are underestimated (Table 4). Iso1 is almost degenerate with the global minimum at the PBE0 level, though it is higher in energy by 8.8 kcal/mol at the CCSD(T) level. The calculated $VDE_1$ for Iso1 is 2.07 eV at the CCSD(T) level. There are no discernible PES signals in the low binding energy range, which rules out the presence of Iso1 in the cluster beam. The 3D Iso2 is 5.0 kcal/mol higher in energy than the global minimum, but it becomes degenerate with the global minimum at the CCSD(T) level. The computed $VDE_1$ of Iso2 is 3.02 eV at the CCSD(T) level. Careful examination of the photoelectron spectrum of $BiB_6^-$ (Figure 1) indicates very weak signals around ∼3.3 eV between bands X and A. This weak feature could suggest the presence of Iso2 in the cluster beam as a minor component.

The calculated VDEs at the PBE0 level for higher binding energy detachment channels of the $C_1$ global minimum are given in Table 1 and marked in Figure 1 by the vertical bars. The first PES band (X) is due to detachment of an electron from the HOMO (27a), which is an in-plane $\sigma$ MO on the $B_6$ moiety (Figure S2). The removal of an electron from the 27a orbital results in a structural change from the quasi-planar anion ($C_1$) to a perfect planar neutral $BiB_6$ ($C_s$). The spectral width of band X is consistent with the geometry change between the ground state of the anion and that of the neutral. Electron detachment from the HOMO−1 (26a) gives a computed VDE of 3.78 eV, in good agreement with the measured VDE of band A at 3.65 eV. The 26a orbital is a $\pi$ MO (Figure S2), consistent with the observed vibrational progression, which is likely due to a symmetric B−B vibrational mode. Electron detachment from the HOMO−2 (25a) results in a theoretical VDE of 4.20 eV, again in good agreement with the measured VDE of band B at 4.26 eV. The 25a orbital is an in-plane $\sigma$ MO, involving in B−B bonding and Bi−B bonding. Significant structural changes are expected upon detachment of a 25a electron, consistent with the broad B band in the photoelectron spectrum (Figure 1). The theoretical results for the elongated $C_1$ structure are in excellent agreement with the experimental observations, providing considerable credence for it to be the global minimum of $BiB_6^-$.

*5.1.2. $BiB_7^-$.* The computed ADE/$VDE_1$ for the global minimum of $BiB_7^-$ are 2.75/3.18 eV at the CCSD(T) level (Table 4). Even though the computed ADE seems to be underestimated in comparison to the experimental value (3.03 eV), the computed $VDE_1$ is in good agreement with the experimental value of 3.21 eV. The calculated $VDE_1$ of 2.83 eV for Iso1 at the CCSD(T) level is in good agreement with the minor feature at 2.84 eV. Higher binding energy detachment features from the minor isomer are likely buried in the spectral features of the global minimum.

As shown in Figure 5, the global minimum of neutral $BiB_7$ is a half-sandwich 3D structure, and it cannot be reached from photodetachment of the planar anion global minimum. The final states of the photodetachment should be those involving Iso1 of neutral $BiB_7$ (Figure 5B), which is a 2D structure but nonplanar. The substantial geometry change from the global minimum of $BiB_7^-$ to Iso1 of $BiB_7$ is consistent with the broad spectral width of band X (Figure 2). Band X is derived from electron detachment of the $2a_2$ SOMO (Figure S3), which is a bonding $\pi$ orbital. As will be shown below, the removal of the $\pi$ electron in the $2a_2$ orbital makes the neutral 2D $BiB_7$ an antiaromatic system, consistent with the large geometry change and the fact that it is no longer the global minimum on the neutral potential energy surface. The next detachment channel takes place from the $4b_1$ HOMO, which gives rise to a high-spin ($^3B_1$) and a low-spin ($^1B_1$) final state. The calculated VDEs for these two final states, 3.52 and 3.90 eV (Table 2), are in good agreement with the measured VDEs of band A (3.42 eV) and band B (3.81 eV). Detachment from the $9b_2$ HOMO−1 also results in a high-spin ($^3B_2$) and a low-spin ($^1B_2$) final state. The calculated VDE for the $^3B_2$ final state (3.63 eV) is consistent with the unresolved shoulder at ∼3.5 eV of the A band, whereas that for the $^1B_2$ (4.07 eV) agrees well with band C (4.04 eV). Finally, the detachment from the $15a_1$ HOMO−2 leads to two final states with different spins ($^3A_1$ and $^1A_1$) and similar VDEs (4.46 and 4.48 eV), which are in good accord with the experimental VDEs of band D at 4.39 eV and band E at 4.47 eV, respectively. Hence, the congested photoelectron spectrum of $BiB_7^-$ is a direct consequence of the open-shell nature of its global minimum. The good agreement between experiment and theory provides strong evidence for the $C_{2v}$ ($^2A_2$) global minimum of $BiB_7^-$.

Even though Iso1 is a relatively high energy isomer for $BiB_7^-$, it is apparently present as a minor component experimentally. The geometry of the global minimum and that of Iso1 are in fact very similar. The major difference is the much larger separation between the two B atoms that are bonded to the Bi atom or the B−Bi−B bond angle in Iso1. As shown in Figure S3, the SOMO ($2a_2$) of the global minimum is a $\pi$ orbital on the $B_7$ moiety, while the HOMO ($4b_1$) is a $\pi$ orbital involving B−Bi−B bonding. Iso1 can be viewed as a consequence of promoting an electron from the $4b_1$ orbital to the $2a_1$ orbital, thus weakening the B−Bi−B bond and resulting in a large B−Bi−B bond angle.

*5.1.3. $BiB_8^-$.* The calculated ADE/$VDE_1$ for the global minimum of $BiB_8^-$ are 3.13/3.19 eV at the CCSD(T) level of theory (Table 4), in excellent agreement with the experimental values of 3.07/3.13 eV. The global minimum of neutral $BiB_8$ is also a 3D half-sandwich type structure similar to that of $BiB_7$, except that the Bi atom is off center and only interacts with


https://doi.org/10.1021/acs.jpca.1c05846
J. Phys. Chem. A 2021, 125, 6751−6760

part of the $B_8$ plane (Figure 5C). Iso1 of $BiB_8$ is similar to the global minimum of $BiB_8^-$ and should be the final state of photodetachment from the $2a_2$ HOMO (Figure S4). There is very little structure change between the $C_{2v}$ $BiB_8^-$ global minimum and the $C_{2v}$ Iso1 of $BiB_8$, consistent with the sharp X band observed in the photoelectron spectrum (Figure 3). The next detachment channel from the $10b_2$ HOMO−1 gives a computed VDE of 3.78 eV, in good agreement with the broad band A at 3.64 eV (Table 3). The $10b_2$ orbital is an in-plane $\sigma$ MO. Electron detachment from this orbital is expected to induce structural changes in the $B_8$ moiety, consistent with the broad band A. The next detachment channel is from the $4b_1$ HOMO−2 with a computed VDE of 4.10 eV, in excellent agreement with the measured VDE of band B at 4.18 eV. The $4b_1$ orbital is a $\pi$ MO. Electron detachment from the $4b_1$ orbital is expected to activate the totally symmetric mode involving the Bi atom, in agreement with the simple vibrational progression observed for band B. Overall, the theoretical results are in excellent agreement with the experimental data, confirming the closed-shell planar $C_{2v}$ global minimum of $BiB_8^-$.

The lowest-lying isomer of $BiB_8^-$ is a 3D structure with a triplet state and $C_{6v}$ symmetry (Figure 5C). The computed $VDE_1$ for the $C_{6v}$ isomer is 3.78 eV (Table 4), which would be buried under band A of the global minimum (Figure 3) if it was present in the cluster beam. Iso2 of $BiB_8^-$ is also a triplet state with $C_s$ symmetry. The calculated VDE1 of 2.74 eV at the CCSD(T) level is in good agreement with the weak PES feature at ∼2.7 eV in the photoelectron spectrum of $BiB_8^-$ (Table 4). However, Iso3, which is close in energy to Iso2, also gives a computed $VDE_1$ (2.88 eV) that could correspond to the weak feature at ∼2.7 eV. Regardless, the low binding energy feature in the spectrum of $BiB_8^-$ (Figure 3) is very weak, and the minor isomer in the cluster beam is almost negligible, in accord with their relatively high energies (Figure 5C).

**5.2. Chemical Bonding in $BiB_n^-$ ($n$ = 6−8).** Because of the relativistic effects,[59] the $6s^2$ electrons of Bi are significantly stabilized and do not actively participate in chemical bonding. Thus, only the 6p orbitals are involved in bonding in Bi compounds without sp hybridization. A $6s^2$ lone pair is found in all Bi−B binary clusters reported previously.[34−36] We have analyzed the bonding in $BiB_n^-$ ($n$ = 6−8) using AdNDP, as shown in Figures 6−8, respectively. A $6s^2$ lone pair is found in each case, whereas the $6p_x$ and $6p_y$ orbitals form two Bi−B $\sigma$ bonds and the $6p_z$ orbital participates in $\pi$ bonding with the $B_n$ moiety.

*5.2.1. $BiB_6^-$.* The AdNDP results for $BiB_6^-$ are shown in Figure 6. In addition to the expected 1c−2e $6s^2$ lone pair on Bi, we found seven 2c−2e $\sigma$ bonds (five B−B and two Bi−B bonds) on the periphery of the 2D $BiB_6^-$ cluster, two 3c−2e delocalized $\sigma$ bonds, and two delocalized $\pi$ bonds. Each of the delocalized $\sigma$ and $\pi$ systems fulfills the $4N$ electron counting rule for antiaromaticity, making $BiB_6^-$ doubly antiaromatic. The elongated shape and nonplanarity of $BiB_6^-$ are consistent with the double antiaromaticity.

*5.2.2. $BiB_7^-$.* The AdNDP results for the global minimum of $BiB_7^-$ (Figure 7) reveal the expected $6s^2$ lone pair on Bi, seven 2c−2e peripheral $\sigma$ bonds (five B−B and two Bi−B bonds), three delocalized $\sigma$ bonds, and three delocalized $\pi$ bonds. However, one of the $\pi$ bonds is a single-electron bond because $BiB_7^-$ is open-shell. The six delocalized $\sigma$ electrons render $BiB_7^-$ $\sigma$ aromatic. Even though there are only five delocalized $\pi$ electrons, $BiB_7^-$ should still be considered $\pi$ aromatic on the basis of its planarity. Upon removing the SOMO $\pi$ electron in $BiB_7^-$, the resulting $BiB_7$ neutral becomes antiaromatic, consistent with its out-of-plane distortion (Iso1, Figure 5B). The relatively large electron binding energy of $BiB_7^-$ is also consistent with the $\pi$ aromatic interpretation. The ADE of $BiB_7^-$ is almost the same as that of $BiB_8^-$ (Table 4), both derived from removing a $\pi$ electron (SOMO for $BiB_7^-$ and HOMO for $BiB_7^-$). Adding an electron to $BiB_7^-$ would make a perfectly doubly aromatic $BiB_7^{2-}$ species. However, removing a $\pi$ electron from $BiB_7^{2-}$ probably weakens the $\pi$ aromaticity in $BiB_7^-$ but does not seem to destroy it. This is also confirmed by the electron detachment from the $\pi$ HOMO of $BiB_8^-$. There is little structural change in the resulting $BiB_8$ neutral (Iso1 in Figure 5C).

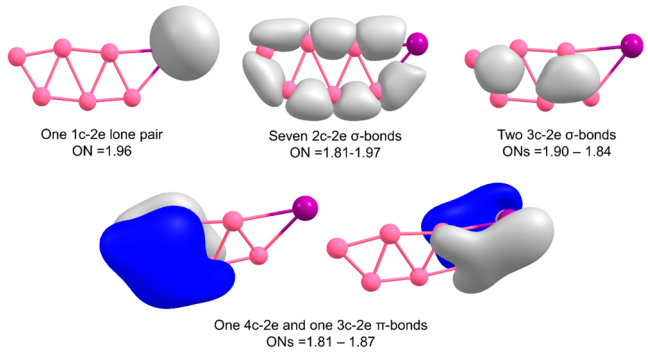


**Figure 6.** AdNDP bonding analysis for $BiB_6^-$. ON stands for occupation number.

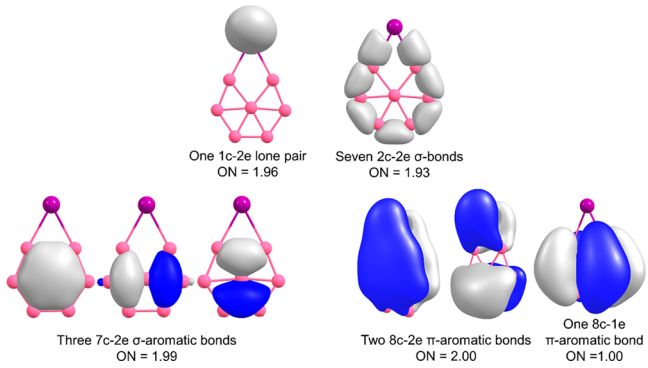


**Figure 7.** AdNDP bonding analysis of $BiB_7^-$. ON stands for occupation number.

*5.2.3. $BiB_8^-$.* The bonding picture of $BiB_8^-$ is similar to that of $BiB_7^-$ but more straightforward because it is a closed-shell system. The AdNDP analyses (Figure 8) reveal the $6s^2$ lone pair of the Bi atom, eight 2c−2e peripheral $\sigma$ bonds (six B−B and two Bi−B bonds), three delocalized $\sigma$ bonds, and three delocalized $\pi$ bonds. Each of the delocalized $\sigma$ and $\pi$ systems satisfies the $4N$ + 2 Hückel rule for aromaticity, rendering $BiB_8^-$ doubly aromatic. The double aromaticity in $BiB_8^-$ is reminiscent of that in the bare closed-shell $B_8^{2-}$ system.[60] In fact, the $B_8$ moiety in $BiB_8^-$ is very similar to the bare boron cluster with little structural distortion.[58]

**5.3. Chemical Bonding in the Global Minima of Neutral $BiB_7$ and $BiB_8$.** In all the global minimum planar structures of $BiB_n^-$ ($n$ = 6−8), the Bi atom can be viewed as a trivalent "big nitrogen", engaging in covalent bonding with the planar boron moiety by using its three 6p orbitals while the $6s^2$ electrons are inert and remain as a lone pair. In each case, Bi


https://doi.org/10.1021/acs.jpca.1c05846
J. Phys. Chem. A 2021, 125, 6751−6760

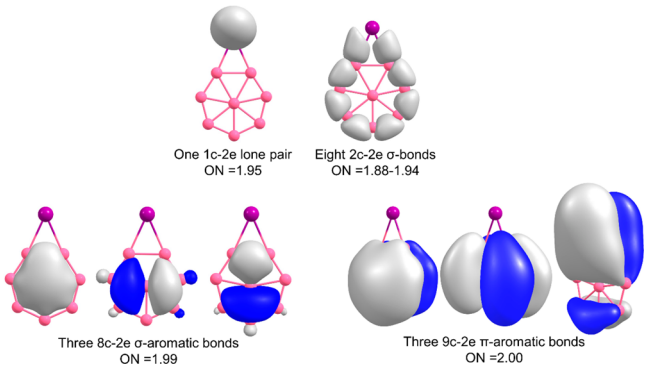


**Figure 8.** AdNDP bonding analysis of $BiB_8^-$. ON stands for occupation number.

forms two localized Bi−B 2c−2e $\sigma$ bonds by using its $6p_x$ and $6p_y$ orbitals and participates in multicenter $\pi$-bonding with its $6p_z$ orbital. The large atomic radius of the Bi atom hinders its insertion into the periphery of the planar boron clusters, in contrast to that observed in carbon- or Al-doped boron clusters.[61−65] Thus, in all cases the Bi atom is side-bonded to the planar boron moiety with relatively small perturbation to their structures compared to the respective bare boron clusters.[56−58] However, except for neutral $BiB_6$, the global minima of neutral $BiB_7$ and $BiB_8$ become 3D half-sandwich-type structures, while the planar structures derived from the anions become higher energy isomers, as shown in Figure 5. In these cases, the electronic stability and aromaticity of the respective boron clusters seem to dictate the structures and stability of neutral $BiB_7$ and $BiB_8$, in which the metallic bonding property of Bi is revealed.

*5.3.1. Half-Sandwich $BiB_7$.* The global minimum of neutral $BiB_7$ is closed-shell with a $C_{6v}$ ($^1A_1$) half-sandwich structure (Figure 5B). As shown in Figure 9, chemical bonding analyses

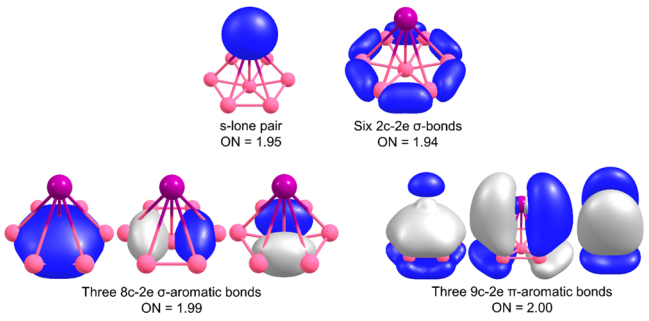


**Figure 9.** AdNDP bonding analysis for the half-sandwich global minimum of neutral $BiB_7$. ON stands for the occupation number.

using AdNDP reveal that the $C_{6v}$ $BiB_7$ possesses a $6s^2$ lone pair, six 2c−2e $\sigma$ bonds on the periphery of the $B_7$ moiety, three delocalized $\sigma$ bonds, and three delocalized $\pi$ bonds. The global minimum of $B_7^-$ is a triplet with two unpaired electrons and a $C_{6v}$ structure.[57] The closed-shell $B_7^{3-}$ species is known to be doubly aromatic and forms half-sandwich type clusters, first observed in $PrB_7$ and recently in $B_7$−B−$BO^-$.[22,23] It has been used to design several binary clusters computationally.[66−68] Thus, the stability of the $C_{6v}$ $BiB_7$ is a consequence of the high stability of the doubly aromatic $B_7^{3-}$ species; the three 6p electrons participate in the $\pi$ bonding with the $B_7$ moiety to fulfill the $\pi$ aromaticity. Thus, the $C_{6v}$ $BiB_7$ can be viewed as $[\eta^7\text{-}B_7^{3-}][Bi^{3+}]$, where the metallic bonding property of Bi is manifested.

Electron detachment from the planar global minimum of the $BiB_7^-$ anion and subsequent optimization of the resulting neutral $BiB_7$ give the low-lying neutral $C_s$ isomer, which is 16.3 kcal/mol higher in energy than the $C_{6v}$ global minimum (Figure 5). While the $C_s$ structure is still $\sigma$-aromatic, it becomes $\pi$-antiaromatic because the electron is detached from the $\pi$ SOMO, leaving only four electrons in the closed-shell neutral. The out-of-plane distortion of the $C_s$ $BiB_7$ isomer is consistent with the $\pi$ antiaromaticity. Both the extraordinary stability of the aromatic $C_{6v}$ structure and the antiaromaticity of the $C_s$ structure results in the large energy separation (16.3 kcal/mol) between the two structures of neutral $BiB_7$.

*5.3.2. Half-Sandwich $BiB_8$.* The global minimum of neutral $BiB_8$ is a half-sandwich-like structure with $C_s$ symmetry, in which the Bi atom is off-center and only interacts with part of the $B_8$ plane (Figure 5C). The AdNDP bonding analysis reveals a $6s^2$ lone pair, a single 6p electron, seven 2c−2e $\sigma$ bonds on the periphery of the $B_8$ moiety, three delocalized $\sigma$ bonds, and three delocalized $\pi$ bonds, as shown in Figure 10.

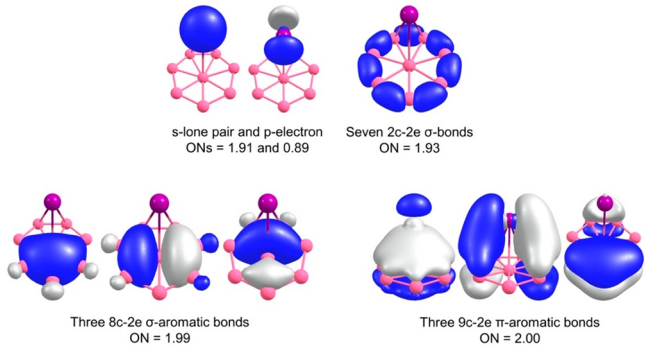


**Figure 10.** AdNDP bonding analysis for the half-sandwich global minimum of neutral $BiB_8$. ON stands for the occupation number.

The two delocalized $\sigma$ and $\pi$ systems make $BiB_8$ doubly aromatic. Neutral $B_8$ is known to be doubly aromatic with a triplet state and $D_{7h}$ symmetry,[58] whereas the closed-shell $B_8^{2-}$ is also doubly aromatic and highly stable.[60] Thus, similar to the $C_{6v}$ $BiB_7$, it is the highly stable doubly aromatic $B_8^{2-}$ ligand that favors the half-sandwich-like structure for $BiB_8$, which can be viewed as $[\eta^5\text{-}B_8^{2-}][Bi^{2+}]$ (Figure 5C). Thus, the Bi atom transfers two electrons to the $B_8$ moiety to fulfill its double aromaticity, leaving it in a rare oxidation state of +II.

Electron detachment from the $C_{2v}$ global minimum of the $BiB_8^-$ anion and subsequent reoptimization result in the low-lying isomer of neutral $BiB_8$ (Iso1, Figure 5C), which has very little structure distortion relative to the anion. Apparently, the removal of a $\pi$ electron from $BiB_8^-$ (HOMO, Figure S5) may have weakened its aromaticity but does not destroy it, similar to the five-$\pi$-electron situation in the planar global minimum of $BiB_7^-$. The lingering aromaticity in the five-electron $C_{2v}$ $BiB_8$ can also be glimpsed by the fact that it is only 5.6 kcal/mol higher in energy than the half-sandwich-like global minimum. This observation also indirectly confirms the $\pi$ aromaticity in the five-$\pi$-electron global minimum of $BiB_7^-$ and the antiaromatic behavior of the corresponding neutral $BiB_7$, which is 16.3 kcal/mol higher in energy than the half-sandwich global minimum of $BiB_7$.



https://doi.org/10.1021/acs.jpca.1c05846
J. Phys. Chem. A 2021, 125, 6751−6760

## 6. CONCLUSIONS

We report a combined photoelectron spectroscopy and theoretical study of a series of Bi-doped boron clusters, $BiB_n^-$ ($n$ = 6−8). Well-resolved photoelectron spectra are obtained for all three clusters and are used to understand their structures and bonding. All three clusters are found to be planar with the Bi atom side-bonded to the boron cluster moiety. The global minimum of $BiB_6^-$ has an elongated double-chain boron motif with a terminal Bi atom, consistent with its double antiaromaticity. The global minima of $BiB_7^-$ and $BiB_8^-$ consist of a wheel-like boron motif with the Bi atom bonded to its edge, and both are doubly aromatic. The Bi atom engages in covalent bonding by using its three 6p orbitals with the planar boron moieties, forming two Bi−B $\sigma$ bonds with the $6p_x$ and $6p_y$ orbitals while the $6p_z$ orbital participates in delocalized $\pi$ bonding. In the $BiB_n$ neutrals, $BiB_6$ has a planar global minimum similar to its anion, but the global minima of both $BiB_7$ and $BiB_8$ are found to have half-sandwich-type 3D structures as a result of the high stability of the doubly aromatic $C_{6v}$ $B_7^{3-}$ and $D_{7h}$ $B_8^{2-}$ species, where the Bi atom primarily engages in ionic bonding.

## ■ ASSOCIATED CONTENT

### Supporting Information

The Supporting Information is available free of charge at https://pubs.acs.org/doi/10.1021/acs.jpca.1c05846.

Additional low-lying structures for $BiB_n^-$ ($n$ = 6−8), valence molecular orbital for the global minima of $BiB_n^-$, and the coordinates of the global minima of $BiB_n^-$ and $BiB_n$ (PDF)

## ■ AUTHOR INFORMATION


### Corresponding Authors

**Lai-Sheng Wang** − *Department of Chemistry, Brown University, Providence, Rhode Island 02912, United States;* orcid.org/0000-0003-1816-5738; Email: lai-sheng_wang@brown.edu

**Alexander I. Boldyrev** − *Department of Chemistry and Biochemistry, Utah State University, Logan, Utah 84322, United States;* orcid.org/0000-0002-8277-3669; Email: a.i.boldyrev@usu.edu

**Dao-Fu Yuan** − *Department of Chemistry, Brown University, Providence, Rhode Island 02912, United States;* orcid.org/0000-0001-8461-6889; Email: daofu_yuan@brown.edu

### Authors

**Wei-Jia Chen** − *Department of Chemistry, Brown University, Providence, Rhode Island 02912, United States*

**Maksim Kulichenko** − *Department of Chemistry and Biochemistry, Utah State University, Logan, Utah 84322, United States*

**Hyun Wook Choi** − *Department of Chemistry, Brown University, Providence, Rhode Island 02912, United States*

**Joseph Cavanagh** − *Department of Chemistry, Brown University, Providence, Rhode Island 02912, United States*

Complete contact information is available at: https://pubs.acs.org/10.1021/acs.jpca.1c05846

### Author Contributions

W.-J.C. and M.K. contributed equally to this work.


### Notes

The authors declare no competing financial interest.

## ■ ACKNOWLEDGMENTS

The experiment done at Brown University was supported by the National Science Foundation (CHE-2053541). Computational resources are supported by the Center for High Performance Computing at the University of Utah.

## ■ REFERENCES


(1) Lipscomb, W. N. The boranes and their relatives. *Science* **1977**, *196*, 1047−1055.

(2) Jemmis, E. D.; Prasad, D. L. V. K. Icosahedral $B_{12}$, macropolyhedral boranes,-rhombohedral boron and boron-rich solids. *J. Solid State Chem.* **2006**, *179*, 2768−2774.

(3) Oganov, A. R.; Chen, J.; Gatti, C.; Ma, Y.; Ma, Y.; Glass, C. W.; Liu, Z.; Yu, T.; Kurakevych, O. O.; Solozhenko, V. L. Ionic high-pressure form of elemental boron. *Nature* **2009**, *457*, 863−867.

(4) Albert, B.; Hillebrecht, H. Boron: Elementary challenge for experimenters and theoreticians. *Angew. Chem., Int. Ed.* **2009**, *48*, 8640−8668.

(5) Alexandrova, A. N.; Boldyrev, A. I.; Zhai, H. J.; Wang, L. S. All-boron aromatic clusters as potential new inorganic ligands and building blocks in chemistry. *Coord. Chem. Rev.* **2006**, *250*, 2811−2866.

(6) Oger, E.; Crawford, N. R. M.; Kelting, R.; Weis, P.; Kappes, M. M.; Ahlrichs, R. Boron cluster cations: transition from planar to cylindrical structures. *Angew. Chem., Int. Ed.* **2007**, *46*, 8503−8506.

(7) Sergeeva, A. P.; Popov, I. A.; Piazza, Z. A.; Li, W. L.; Romanescu, C.; Wang, L. S.; Boldyrev, A. I. Understanding boron through size-selected clusters: Structure, chemical bonding, and fluxionality. *Acc. Chem. Res.* **2014**, *47*, 1349−1358.

(8) Wang, L. S. Photoelectron spectroscopy of size-selected boron clusters: from planar structures to borophenes and borospherenes. *Int. Rev. Phys. Chem.* **2016**, *35*, 69−142.

(9) Jian, T.; Chen, X.; Li, S. D.; Boldyrev, A. I.; Li, J.; Wang, L. S. Probing the structures and bonding of size-selected boron and doped-boron clusters. *Chem. Soc. Rev.* **2019**, *48*, 3550−3591.

(10) Pan, S.; Barroso, J.; Jalife, S.; Heine, T.; Asmis, K. R.; Merino, G. Fluxional boron clusters: from thoery to reality. *Acc. Chem. Res.* **2019**, *52*, 2732−2744.

(11) Piazza, Z. A.; Hu, H. S.; Li, W. L.; Zhao, Y. F.; Li, J.; Wang, L. S. Planar hexagonal $B_{36}$ as a potential basis for extended single-atom layer boron sheets. *Nat. Commun.* **2014**, *5*, 3113.

(12) Mannix, A. J.; Zhou, X. F.; Kiraly, B.; Wood, J. D.; Alducin, D.; Myers, B. D.; Liu, X.; Fisher, B. L.; Santiago, U.; Guest, J. R.; et al. Synthesis of borophenes: Anisotropic, two-dimensional boron polymorphs. *Science* **2015**, *350*, 1513.

(13) Feng, B.; Zhang, J.; Zhong, Q.; Li, W.; Li, S.; Li, H.; Cheng, P.; Meng, S.; Chen, L.; Wu, K. Experimental realization of two-dimensional boron sheets. *Nat. Chem.* **2016**, *8*, 563−568.

(14) Zhai, H. J.; Zhao, Y. F.; Li, W. L.; Chen, Q.; Bai, H.; Hu, H. S.; Piazza, Z. A.; Tian, W. J.; Lu, H. G.; Wu, Y. B.; et al. Observation of an all-boron fullerene. *Nat. Chem.* **2014**, *6*, 727−731.

(15) Chen, W. J.; Ma, Y. Y.; Chen, T. T.; Ao, M. Z.; Yuan, D. F.; Chen, Q.; Tian, X. X.; Mu, Y. W.; Li, S. D.; Wang, L. S. $B_{48}^-$: a bilayer boron cluster. *Nanoscale* **2021**, *13*, 3868−3876.

(16) Romanescu, C.; Galeev, T. R.; Li, W. L.; Boldyrev, A. I.; Wang, L. S. Aromatic metal-centered monocyclic boron rings: $Co©B_8^-$ and $Ru©B_9^-$. *Angew. Chem., Int. Ed.* **2011**, *50*, 9334−9337.

(17) Galeev, T. R.; Romanescu, C.; Li, W. L.; Wang, L. S.; Boldyrev, A. I. Observation of the highest coordination number in planar species: decacoordinated $Ta©B_{10}^-$ and $Nb©B_{10}^-$ anions. *Angew. Chem., Int. Ed.* **2012**, *51*, 2101−2105.

(18) Romanescu, C.; Galeev, T. R.; Li, W. L.; Boldyrev, A. I.; Wang, L. S. Transition-metal-centered monocyclic boron wheel clusters ($M©B_n$): A new class of aromatic borometallic compounds. *Acc. Chem. Res.* **2013**, *46*, 350−358.

(19) Popov, I. A.; Jian, T.; Lopez, G. V.; Boldyrev, A. I.; Wang, L. S. Cobalt-centred boron molecular drums with the highest coordination number in the $CoB_{16}^-$ cluster. *Nat. Commun.* **2015**, *6*, 8654.
(20) Li, W. L.; Jian, T.; Chen, X.; Chen, T. T.; Lopez, G. V.; Li, J.; Wang, L. S. The planar $CoB_{18}^-$ cluster as a motif for metallo-borophenes. *Angew. Chem., Int. Ed.* **2016**, *55*, 7358−7363.
(21) Li, W. L.; Chen, X.; Jian, T.; Chen, T. T.; Li, J.; Wang, L. S. From planar boron clusters to borophenes and metalloborophenes. *Nat. Rev. Chem.* **2017**, *1*, 0071.
(22) Chen, T. T.; Li, W. L.; Jian, T.; Chen, X.; Li, J.; Wang, L. S. $PrB_7^-$: A praseodymium-doped boron cluster with a $Pr^{II}$ center coordinated by a doubly aromatic planar $\eta^7$-$B_7^{3-}$ ligand. *Angew. Chem., Int. Ed.* **2017**, *56*, 6916−6920.
(23) Tian, W. J.; Chen, W. J.; Yan, M.; Li, R.; Wei, Z. H.; Chen, T. T.; Chen, Q.; Zhai, H. J.; Li, S. D.; Wang, L. S. Transition-metal-like bonding behaviors of a boron atom in a boron-cluster boronyl complex $[(\eta^7\text{-}B_7)\text{-}B\text{-}BO]^-$. *Chem. Sci.* **2021**, *12*, 8157−8164.
(24) Li, W. L.; Chen, T. T.; Xing, D. H.; Chen, X.; Li, J.; Wang, L. S. Observation of highly stable and symmetric lanthanide octa-boron inverse sandwich complexes. *Proc. Natl. Acad. Sci. U. S. A.* **2018**, *115*, E6972.
(25) Chen, T. T.; Li, W. L.; Li, J.; Wang, L. S. $[La(\eta^x\text{-}B_x)La]^-$ ($x$ = 7−9): a new class of inverse sandwich complexes. *Chem. Sci.* **2019**, *10*, 2534−2542.
(26) Chen, T. T.; Li, W. L.; Chen, W. J.; Yu, X. H.; Dong, X. R.; Li, J.; Wang, L. S. Spherical trihedral metallo-borospherenes. *Nat. Commun.* **2020**, *11*, 2766.
(27) Mohan, R. Green bismuth. *Nat. Chem.* **2010**, *2*, 336−336.
(28) Ramler, J.; Lichtenberg, C. Bismuth species in the coordination sphere of transition metals: synthesis, bonding, coordination chemistry, and reactivity of molecular complexes. *Dalton Trans.* **2021**, *50*, 7120−7138.
(29) Zhang, Y.; Liu, Y.; Xu, Z.; Ye, H.; Yang, Z.; You, J.; Liu, M.; He, Y.; Kanatzidis, M. G.; Liu, S. Nucleation-controlled growth of superior lead-free perovskite $Cs_3Bi_2I_9$ single-crystals for high-performance X-ray detection. *Nat. Commun.* **2020**, *11*, 2304.
(30) Salvador, J. A. R.; Figueiredo, S. A. C.; Pinto, R. M. A.; Silvestre, S. M. Bismuth compounds in medicinal chemistry. *Future Med. Chem.* **2012**, *4*, 1495−1523.
(31) Madouri, D.; Ferhat, M. How do electronic properties of conventional III−V semiconductors hold for the III−V boron bismuth BBi compound? *Phys. Status Solidi B* **2005**, *242*, 2856−2863.
(32) Cui, S.; Feng, W.; Hu, H.; Feng, Z.; Wang, Y. First principles studies of phase stability, electronic and elastic properties in BBi compound. *Comput. Mater. Sci.* **2010**, *47*, 968−972.
(33) Bagci, S.; Yalcin, B. G. Structural, mechanical, electronic and optical properties of BBi, BP and their ternary alloys $BBi_{1-x}P_x$. *J. Phys. D: Appl. Phys.* **2015**, *48*, 475304.
(34) Jian, T.; Lopez, G. V.; Wang, L. S. Photoelectron spectroscopy of $BiAu^-$ and $BiBO^-$: Further evidence of the analogy between Au and boronyl. *J. Phys. Chem. B* **2016**, *120*, 1635−1640.
(35) Jian, T.; Cheung, L. F.; Chen, T. T.; Wang, L. S. Bismuth−boron multiple bonding in $BiB_2O^-$ and $Bi_2B^-$. *Angew. Chem., Int. Ed.* **2017**, *56*, 9551−9555.
(36) Cheung, L. F.; Czekner, J.; Kocheril, G. S.; Wang, L. S. High resolution photoelectron imaging of boron-bismuth binary clusters: $Bi_2B_n^-$ ($n$ = 2−4). *J. Chem. Phys.* **2019**, *150*, 064304.
(37) Wang, L. S.; Cheng, H. S.; Fan, J. Photoelectron spectroscopy of size□selected transition metal clusters: $Fe_n^-$, $n$ = 3−24. *J. Chem. Phys.* **1995**, *102*, 9480−9493.
(38) Akola, J.; Manninen, M.; Hakkinen, H.; Landman, U.; Li, X.; Wang, L. S. Photoelectron spectra of aluminum cluster anions: temperature effects and ab initio simulations. *Phys. Rev. B: Condens. Matter Mater. Phys.* **1999**, *60*, R11297−R11300.
(39) Huang, W.; Wang, L. S. Probing the 2D to 3D structural transition in gold cluster anions using argon tagging. *Phys. Rev. Lett.* **2009**, *102*, 153401.
(40) Zhai, H.; Ha, M. A.; Alexandrova, A. N. AFFCK: Adaptive force-field-assisted ab initio coalescence kick method for global minimum search. *J. Chem. Theory Comput.* **2015**, *11*, 2385−2393.
(41) Adamo, C.; Barone, V. Toward reliable density functional methods without adjustable parameters: The PBE0 model. *J. Chem. Phys.* **1999**, *110*, 6158−6170.
(42) Dunning, T. H. Gaussian basis sets for use in correlated molecular calculations. I. The atoms boron through neon and hydrogen. *J. Chem. Phys.* **1989**, *90*, 1007−1023.
(43) Frisch, M. J.; Trucks, G. W.; Schlegel, H. B.; Scuseria, G. E.; Robb, M. A.; Cheeseman, J. R.; Scalmani, G.; Barone, V.; Petersson, G. A.; Nakatsuji, H.; et al. *Gaussian 16*, Revision C.01; Gaussian, Inc.: 2016.
(44) Purvis, G. D.; Bartlett, R. J. A full coupled□cluster singles and doubles model: The inclusion of disconnected triples. *J. Chem. Phys.* **1982**, *76*, 1910−1918.
(45) Weigend, F. Accurate Coulomb-fitting basis sets for H to Rn. *Phys. Chem. Chem. Phys.* **2006**, *8*, 1057−1065.
(46) Zubarev, D. Y.; Boldyrev, A. I. Developing paradigms of chemical bonding: adaptive natural density partitioning. *Phys. Chem. Chem. Phys.* **2008**, *10*, 5207−5217.
(47) Zubarev, D. Y.; Boldyrev, A. I. Revealing intuitively assessable chemical bonding patterns in organic aromatic molecules via adaptive natural density partitioning. *J. Org. Chem.* **2008**, *73*, 9251−9258.
(48) Zubarev, D. Y.; Averkiev, B. B.; Zhai, H. J.; Wang, L. S.; Boldyrev, A. I. Aromaticity and antiaromaticity in transition-metal systems. *Phys. Chem. Chem. Phys.* **2008**, *10*, 257−267.
(49) Min, X.; Popov, I. A.; Pan, F.-X.; Li, L. J.; Matito, E.; Sun, Z. M.; Wang, L. S.; Boldyrev, A. I. All-metal antiaromaticity in $Sb_4$-type lanthanocene anions. *Angew. Chem., Int. Ed.* **2016**, *55*, 5531−5535.
(50) Kulichenko, M.; Fedik, N.; Steglenko, D.; Minyaev, R. M.; Minkin, V. I.; Boldyrev, A. I. Periodic F-defects on the MgO surface as potential single-defect catalysts with non-linear optical properties. *Chem. Phys.* **2020**, *532*, 110680.
(51) Fedik, N.; Kulichenko, M.; Steglenko, D.; Boldyrev, A. I. Can aromaticity be a kinetic trap? Example of mechanically interlocked aromatic [2−5]catenanes built from cyclo[18]carbon. *Chem. Commun.* **2020**, *56*, 2711−2714.
(52) Kulichenko, M.; Boldyrev, A. I. $\sigma$-Aromaticity in the $MoS_2$ Monolayer. *J. Phys. Chem. C* **2020**, *124*, 6267−6273.
(53) Kulichenko, M.; Fedik, N.; Monfredini, A.; Muñoz-Castro, A.; Balestri, D.; Boldyrev, A. I.; Maestri, G. Bottled" spiro-doubly aromatic trinuclear $[Pd_2Ru]^+$ complexes. *Chem. Sci.* **2021**, *12*, 477−486.
(54) Kulichenko, M.; Utenyshev, A. N.; Bozhenko, K. V. Designing molecular electrides from defective unit cells of cubic alkaline earth oxides. *J. Phys. Chem. C* **2021**, *125*, 9564−9570.
(55) Kulichenko, M.; Chen, W. J.; Zhang, Y. Y.; Xu, C. Q.; Li, J.; Wang, L. S. Double $\sigma$-aromaticity in a planar zinc-doped gold cluster: $Au_9Zn^-$. *J. Phys. Chem. A* **2021**, *125*, 4606−4613.
(56) Alexandrova, A. N.; Boldyrev, A. I.; Zhai, H. J.; Wang, L. S.; Steiner, E.; Fowler, P. W. Structure and bonding in $B_6^-$ and $B_6$: planarity and antiaromaticity. *J. Phys. Chem. A* **2003**, *107*, 1359−1369.
(57) Alexandrova, A. N.; Boldyrev, A. I.; Zhai, H. J.; Wang, L. S. Electronic structure, isomerism, and chemical bonding in $B_7^-$ and $B_7$. *J. Phys. Chem. A* **2004**, *108*, 3509−3517.
(58) Zhai, H. J.; Alexandrova, A. N.; Birch, K. A.; Boldyrev, A. I.; Wang, L. S. Hepta□and octacoordinate boron in molecular wheels of eight□and nine□atom boron clusters: observation and confirmation. *Angew. Chem., Int. Ed.* **2003**, *42*, 6004−6008.
(59) Pyykko, P. Relativistic effects in structural chemistry. *Chem. Rev.* **1988**, *88*, 563−594.
(60) Alexandrova, A. N.; Zhai, H.-J.; Wang, L.-S.; Boldyrev, A. I. Molecular wheel $B_8^{2-}$ as a new inorganic ligand. Photoelectron spectroscopy and ab initio characterization of $LiB_8^-$. *Inorg. Chem.* **2004**, *43*, 3552−3554.
(61) Wang, L. M.; Huang, W.; Averkiev, B. B.; Boldyrev, A. I.; Wang, L. S. $CB_7^-$: experimental and theoretical evidence against hyper-


https://doi.org/10.1021/acs.jpca.1c05846
J. Phys. Chem. A 2021, 125, 6751−6760

coordinated planar carbon. *Angew. Chem., Int. Ed.* **2007**, *46*, 4550−4553.
(62) Averkiev, B. B.; Zubarev, D. Y.; Wang, L. M.; Huang, W.; Wang, L. S.; Boldyrev, A. I. Carbon avoids hyper coordination in $CB_6^-$, $CB_6^{2-}$, and $C_2B_5^-$ planar carbon-boron clusters. *J. Am. Chem. Soc.* **2008**, *130*, 9248−9250.
(63) Wang, L. M.; Averkiev, B. B.; Ramilowski, J. A.; Huang, W.; Wang, L. S.; Boldyrev, A. I. Planar to linear structural transition in small boron-carbon mixed clusters: $C_xB_{5-x}^-$ ($x$ = 1−5). *J. Am. Chem. Soc.* **2010**, *132*, 14104−14112.
(64) Romanescu, C.; Sergeeva, A. P.; Li, W. L.; Boldyrev, A. I.; Wang, L. S. Planarization of $B_7^-$ and $B_{12}^-$ clusters by isoelectronic substitution: $AlB_6^-$ and $AlB_{11}^-$. *J. Am. Chem. Soc.* **2011**, *133*, 8646−8653.
(65) Galeev, T. R.; Romanescu, C.; Li, W. L.; Wang, L. S.; Boldyrev, A. I. Valence isoelectronic substitution in the $B_8^-$ and $B_9^-$ molecular wheels by an Al dopant atom: umbrella-like structures of $AlB_7^-$ and $AlB_8^-$. *J. Chem. Phys.* **2011**, *135*, 104301.
(66) Yu, R.; Barroso, J.; Wang, M. H.; Liang, W. Y.; Chen, C.; Zarate, X.; Orozco-Ic, M.; Cui, Z. H.; Merino, G. Structure and bonding of molecular stirrers with formula $B_7M_2^-$ and $B_8M_2$ (M = Zn, Cd, Hg). *Phys. Chem. Chem. Phys.* **2020**, *22*, 12312−12320.
(67) Wang, W.; Wang, J.; Gong, C.; Mu, C.; Zhang, D.; Zhang, X. Designer Mg-Mg and Zn-Zn single bonds facilitated by double aromaticity in the $M_2B_7^-$ (M = Mg, Zn) clsuters. *Chin. J. Chem. Phys.* **2020**, *33*, 578−582.
(68) Wang, Y. J.; Feng, L. Y.; Zhai, H. J. Sandwich-type $Na_6B_7^-$ and $Na_8B_7^+$ clusters: charge-transfer complexes, four-fold p/s aromaticity, and dynamic fluxionality. *Phys. Chem. Chem. Phys.* **2019**, *21*, 18338−18345.


https://doi.org/10.1021/acs.jpca.1c05846
*J. Phys. Chem. A* 2021, 125, 6751−6760